INDERSCIENCE PUBLISHERS
Linking academia, business and industry through research

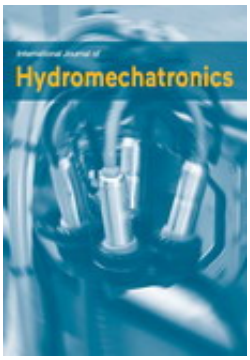

International Journal of Hydromechatronics

ISSN online: 2515-0472 - ISSN print: 2515-0464
https://www.inderscience.com/ijhm

A novel tool condition monitoring based on Gramian angular field and comparative learning

Hongche Wang, Wei Sun, Weifang Sun, Yan Ren, Yuqing Zhou, Qijia Qian, Anil Kumar

DOI: 10.1504/IJHM.2022.10048957

Article History:

Received:	02 April 2022
Accepted:	31 May 2022
Published online:	25 April 2023

A novel tool condition monitoring based on Gramian angular field and comparative learning

Hongche Wang, Wei Sun, Weifang Sun and Yan Ren

College of Mechanical and Electrical Engineering,
Wenzhou University,
Wenzhou, China
Email: Wanghongche@163.com
Email: Sunwei0977@163.com
Email: vincent_suen@126.com
Email: rentingting211@163.com

Yuqing Zhou*

College of Mechanical and Electrical Engineering,
Wenzhou University,
Wenzhou, China
Email: zhouyq@jxnhu.edu.cn
and
College of Mechanical and Electrical Engineering,
Jiaxing Nanhu University,
Jiaxin, China
*Corresponding author

Qijia Qian

Technology Centre,
Wenzhou Ruiming Industrial Co., Ltd.,
Wenzhou, China
Email: 77648750@qq.com

Anil Kumar

College of Mechanical and Electrical Engineering,
Wenzhou University,
Wenzhou, China
Email: anil_taneja86@yahoo.com

Abstract: Accurate tool condition monitoring (TCM) is an important part for ensuring milling quality. However, due to the cost of TCM experiment, there are few labelled and a lot of unlabelled samples in the training set that significantly affect the accuracy of many machine learning models. A novel method based on comparative learning (CL) and Gramian angular field (GAF) is proposed for improving the performance of TCM. The cutting force signals of each channel of all samples (including labelled and unlabelled) collected in

TCM experiment are expanded to grey images by GAF, and combined with other channels to a colour image. Then, these colour images are input to the CL pre-training model to learn features. Finally, the extracted features and the few labelled samples are applied to train the ResNet18 model to obtain excellent classification results. The milling TCM experiments show that the classification precision of the proposed GAF-CL model is above 95% with small labelled samples, which is more than 19% higher than the ImageNet pre-training model.

Keywords: tool condition monitoring; TCM; comparative learning; CL; Gramian angular field; residual network.

Reference to this paper should be made as follows: Wang, H., Sun, W., Sun, W., Ren, Y., Zhou, Y., Qian, Q. and Kumar, A. (2023) 'A novel tool condition monitoring based on Gramian angular field and comparative learning', *Int. J. Hydromechatronics*, Vol. 6, No. 2, pp.93–107.

Biographical notes: Hongche Wang received his BS in Mechanical Design and Manufacturing from Hangzhou Dianzi University, Hangzhou, China, in 2020. He is currently working toward his MS in Mechanical Engineering from Wenzhou University. His research interests include deep learning and fault diagnosis.

Wei Sun received his BS in Mechanical Design and Manufacturing from Linqi University, Linqi, China, in 2020. He is currently working toward his MS in Mechanical Engineering from Wenzhou University. His research interests include tool condition monitoring and machine learning.

Weifang Sun is currently an Associate Professor with the College of Mechanical and Electrical Engineering, Wenzhou University, Wenzhou, China. His research interests include digital information analysis, and artificial intelligence methods.

Yan Ren is currently an Associate Professor with the College of Mechanical and Electrical Engineering, Wenzhou University, Wenzhou, China. Her research interests include mechanical design and optimisation methods.

Yuqing Zhou is currently vice president with the College of Mechanical and Electrical Engineering, Jiaxing Nanhu University, Jiaxing, China, and special-term professor in Wenzhou University, Wenzhou, China. His research interests include tool condition monitoring, mechanical fault diagnosis, and machine learning.

Qijia Qian is currently the Director of the Technology Department, Wenzhou Ruiming Industrial Co., Ltd., Wenzhou, China. His research interests include tool condition monitoring and intelligent manufacturing.

Anil Kumar is currently an Associate Professor with the College of Mechanical and Electrical Engineering, Wenzhou University, Wenzhou, China. His research interests include fault diagnosis and deep learning.

1 Introduction

In the process of material cutting, the tool is in direct contact with the work piece, and the gradual wear of the tool has become an important factor affecting the dimensional accuracy, surface roughness and processing cost of the work piece (Zhou et al., 2020a). Tool wear is a complex process that depends on the experience and subjective judgment of the operator for tool replacement. Replacing the tool too early will reduce the quality of the part and increase the production cost (Hahn and Mechefske, 2021). It is essential to study a reliable and real-time monitoring method to reflect the wear condition of the tool (Vicente et al., 2010). According to the research surface, the establishment of TCM system can reduce 75% of failure downtime (Zhou et al., 2020b), improve 10% ~ 50% of production efficiency (Siddhpura and Paurobally, 2013), and the utilisation rate on machine tool will reach more than 50% (Rehorn et al., 2005).

Today, there are two main methods to monitor tool wear: the direct method and the indirect method. The most typical method of the direct method is a mechanical visual method (Klancnik et al., 2015). Using machine vision tools to directly measure the wear value of the blade has the advantages of intuition and high accuracy, but it needs to stop the machine for measurement, which has low efficiency. Indirect method is the most widely used method. Through the signals collected by sensors in the cutting process of cutting tools under different wear conditions, such as cutting force (Zhu et al., 2021), acoustic emission (Ravindra et al., 1997), vibration (Zhang et al., 2021), use machine learning model to train the input characteristics of the collected signals, and then predict the current collected data (Lei et al., 2021). Li et al. (2019) separated the noise signal by blind source separation method, developed and verified a prediction model. Wu et al. (2017) studied the use of random forest to realise on-line tool wear prediction. Vashishtha et al. (2022) use the improved Shannon entropy maximisation principal component analysis to effectively eliminate the correlation and redundancy of data. Vashishtha et al. (2022) use the improved African vulture optimisation algorithm to extract sensitive features representing different conditions on bearing to improve performance. However, it is also very difficult for these methods to select appropriate features for feature extraction. Therefore, these models need a lot of experiments to verify.

In recent years, the method of deep learning Wang et al. (2019) has been extremely successful in the fields of natural language processing (Li et al., 2020), speech recognition (Hinton et al., 2012) and image recognition (Chan et al., 2014). Deep learning involves reaching the state of end-to-end learning by hierarchical representation of data features and abstract representation of low-level features of high-level features (Zhou et al., 2022), this method Gu et al. (2021) and He et al. (2021) can effectively reduce the dependence on traditional experience in the traditional machine learning model. Deep learning is divided into supervised learning and unsupervised learning, and although supervised learning has a high accuracy rate, it requires a large amount of labelled data for learning (He et al., 2020), and there are also problems such as generalisation errors, false associations, and adversarial attacks (Hahn and Mechefske, 2021). Therefore, in recent years, self-supervised representation, learning on unlabelled data has received more and more attention from scholars. However, the labelled data from the tool milling process are few and expensive, how to use a large amount of unlabelled data to monitor the wear and tear of unsupervised learning milling tools has become a new topic, in the research on unsupervised image classification, Hardsel et al. (2006) first proposed the concept of contrast loss, mapping high-dimensional data to low-dimensional space, and

making similar points in the input closer in space by comparing positive and negative pairs. Chen et al. (2020) proposed SimCLR CL model, adding multi-layer full connection layer and activation layer after the feature extraction network, which solved the problems of slow calculation speed of the model when the dimension of feature vector is high, and achieved good results.

In many practical industrial scenarios, a small number of labelled and a large number of unlabelled samples can be collected for learning, which seriously affects the performance of supervised learning methods. However, when the proportion of labelled data in a large number of datasets is small, the unlabelled data can be fully utilised for self-supervised pre-training through contrastive learning, and contrastive learning has a better classification effect under this structure of datasets. This paper proposes a dimensional image classification algorithm based on CL model in TCM. In the first step, the original time series signals collected by the sensor are imaged into grey images of appropriate size, these images obtained from the three signals are combined through the channel dimension to obtain a 3D colour image as the CL model input. The second step is to input the obtained image without labels into the CL Pre-training model to learn features, the biggest feature of this model is that it can adopt the self-supervised pre-training model under the unlabelled dataset to absorb the prior knowledge distribution of the image itself. In the third step, the extracted features and the few labelled samples are applied to train the ResNet18 model to obtain excellent classification results and compared with other deep learning methods. The paper is divided into the following parts. The second part show GASF, SimCLR CL pre-training model and the overall structure of the model. The third part gives the experimental setup, data analysis and experimental results. Finally, the fourth part summarises this paper.

2 Related work

2.1 GASF

Nowadays, deep learning is widely used as a computer vision. Image data processed by computer vision are two-dimensional data, while data from various sensors are typical data from one-dimensional time series data. However, it is difficult to build a model when processing, time series data, there is no ready-made research and training network to provide one-dimensional time series for training, which has a good effect. Therefore, if the time series or one-dimensional array can be transformed into a two-dimensional image format, and then the deep learning model can be applied for analysis, and has good results, it is a relatively novel application in the field of tool wear condition monitoring. At present, there are many methods to upgrade the dimension of time series. Through genetic algorithm (GA) (Yu and Zhao, 2019), particle swarm optimisation algorithm (PSO) (Higashi and Iba, 2003) and arithmetic optimisation algorithm (AOA) (Chauhan and Vashishtha, 2021), Chauhan et al. (2022) proposed the combination of AOA and slime mould algorithm (SMA) (Jafariasl et al., 2021) to optimise AOA. These methods can obtain the optimal parameters and upgrade the dimension of the signal through phase space reconstruction. In recent years, Wang et al. (2015) proposed three new time series image coding methods: Gramian angular sum/difference field (GASF/GADF), and these methods have been practiced in some papers (Jiang et al., 2021; Zheng et al., 2021).

For GASF, the time series is represented by polar coordinates, select a given time series with length N, and let $X = \{x_1, x_2, x_3 \cdots x_n\}$ be normalised by [–1, 1]. Then, the value of the time series and its corresponding timestamp are respectively expressed as angle Φ_i and radius r.

$$\Phi_i = arcos\left(\tilde{x}_i\right), -1 \le \tilde{x}_i \le 1, \tilde{x}_i \in X \tag{1}$$

$$r = \frac{t_i}{N}\left(t_i \in N\right) \tag{2}$$

In equation (1), the angle corresponding to each timestamp is the arccosine value corresponding to the normalised amplitude of that time point. In equation (2), t_i is the time stamp, and N represents the length of the input time series. As the time increases, the value of each time series will be displayed at different angles and radii on the generated circle, however, when calculating the inner product, different initial points will lead to different inner products between the same sequence points (because their r is different), so a formula is needed, which only depends on the angle. By defining the inner product:

$$\left(\tilde{x}, \tilde{x}\right) = \tilde{x}^T \cdot \tilde{x} - \left(\sqrt{I - \tilde{x}^2}\right)^T \cdot \sqrt{I - \tilde{x}^2} = cos\left(\Phi_i + \Phi_j\right) \tag{3}$$

In equation (3), $\tilde{x}$ is the normalised value of a line of time series, I is the unit row vector [1, 1, 1⋯1]. Becaues of $\tilde{x}\left[cos\left(\Phi_1\right), cos\left(\Phi_2\right), \cdots cos\left(\Phi_n\right)\right]$, their inner product can be transformed into the cosine of the sum of angles. Therefore, in the GASF matrix, each default element is the cosine of the angular sum of the time stamp, the definition formula of GASF is as follows the equation (4).

Figure 1 shows the GASF coding process of time series signals:

a the raw signal extracted by the sensor

b the result of normalising the raw signal

c the normalised signal is expressed in polar coordinates through equations (1) and (2)

d the image is generated by time series signal through equation (3) and (4).

$$T = \begin{bmatrix} cos\left(\Phi_1 + \Phi_1\right) & cos\left(\Phi_1 + \Phi_2\right) & \cdots & cos\left(\Phi_1 + \Phi_n\right) \\ cos\left(\Phi_2 + \Phi_1\right) & cos\left(\Phi_2 + \Phi_2\right) & \cdots & cos\left(\Phi_2 + \Phi_n\right) \\ \vdots & \vdots & \ddots & \vdots \\ cos\left(\Phi_n + \Phi_1\right) & cos\left(\Phi_n + \Phi_2\right) & \cdots & cos\left(\Phi_n + \Phi_n\right) \end{bmatrix} \tag{4}$$

Figure 1 Process of Gramian angular field (a) raw signal (b) normalised signal (c) signal on polar coordinates (d) signal dimension upgrade to picture (see online version for colours)

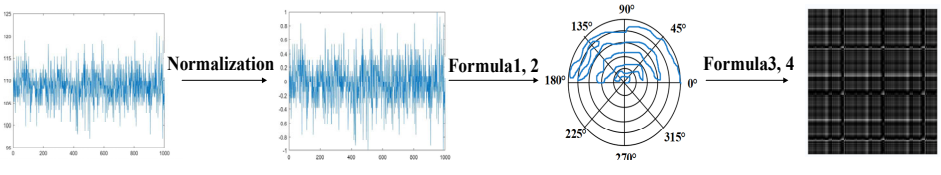

2.2 SimCLR CL pre-training model

The framework of the CL model is shown in Figure 2, including four modules: data augmentation, feature extraction, multi-layer perceptron (MLP) and contrast loss function.

Figure 2 SimCLR framework (see online version for colours)

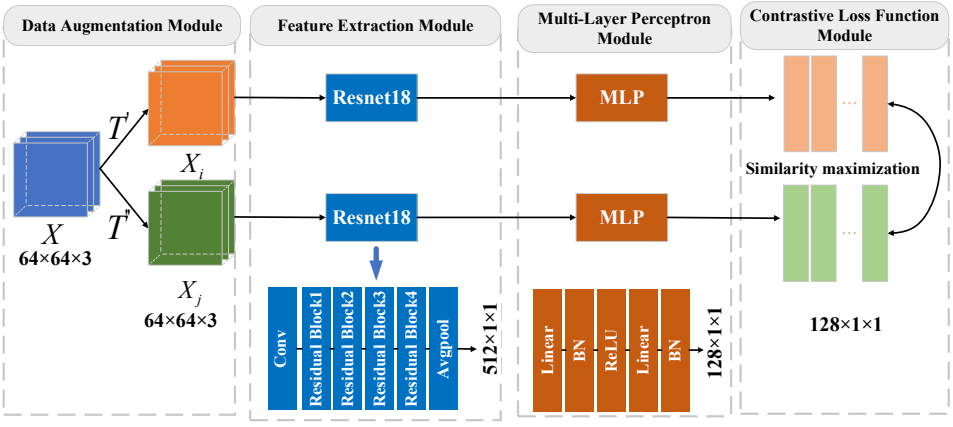

2.2.1 Data augmentation

There are two ways to enhance an image: one involves spatial geometric transformation, such as crop and Horizontal-Flip, and the other involves appearance transformation, such as Colourjitter and grey scale. As shown in Figure 2. In this paper, Gasf method is used to obtain images. Each pixel in the image represents the relationship between each signal, so the data enhancement method of appearance transformation cannot be used, and the form of spatial transformation needs to be used. We ues the T-change is {RandomHorizontalFlip (p = 0.5), RandomResizeCrop (64)}. By default, x_i and x_j generated by a picture through T-change are positive samples, while paired samples generated in other images are negative samples.

2.2.2 Feature extraction

The model needs to input the feature vector, delete the dense layer and leave four residual blocks. The picture is input to the resnet18 network that deletes the dense layer. After each residual block, the feature is extracted adaptively by neural network to obtain the feature vectors of 512×1×1.

2.2.3 Multi-layer perceptron

As shown in Figure 2, the MLP used for projection in this paper adopts two linear layers, and normalisation is used after each linear layer. After the normalisation of the first linear layer, using the ReLU function can better mine relevant features and speed up the fitting of training data. Through the MLP, the high-dimensional features can be reduced to lower features, which can speed up the calculation in the subsequent loss function

calculation. In this paper, the feature output of 512×1×1 is reduced to 128×1×1 through MLP.

2.2.4 Contrast loss function

Specify the size N of a batch size, for the N images of this batch, the images obtained through T-change are recorded as N_1 and N_2, and the features obtained by feature extraction and MLP are Z_1 and Z_2, order $Z = [Z_1; Z_2] \in R^{(2N\times128)}$ (where $[Z_1;Z_2]$ indicates that Z_1 and Z_2 are spliced through columns). Finally, cosine similarity is calculated using the equation (6).

$$Sim(i,j) = \frac{Z_i^T \cdot Z_j}{|Z_i||Z_j|} \tag{6}$$

(where Z_i and Z_j represent columns i and j of matrix Z)

$$l_{i,j} = -log \frac{\exp\left(Sim(i,j)/\tau\right)}{\sum_{k=1}^{2N}{}_{[k\neq i]} \exp\left(Sim(i,j)/\tau\right)} (\tau \in [0,1]) \tag{7}$$

The cross-entropy loss is calculated by equation (7). τ is the temperature parameter which adjusts the attention to difficult samples, the τ is smaller, the more attention is paid to separating this sample from other most similar samples. According to the multiple experiments at τ = 0.07, 0.1, 0.2, 0.5, 1, it can be concluded that the classification accuracy of the model obtained from the experimental dataset is the highest when $a = 0.1$, therefore, in this study, $\tau = 0.1$.

Finally, calculate all losses in n batches through equation (8) and take the average value to obtain the final loss L.

$$L = \frac{1}{2N}\sum_{k=1}^{2N}\left[l(2k-1,2k) + l(2k,2k-1)\right] \tag{8}$$

Figure 3 The overall structure of the model (see online version for colours)

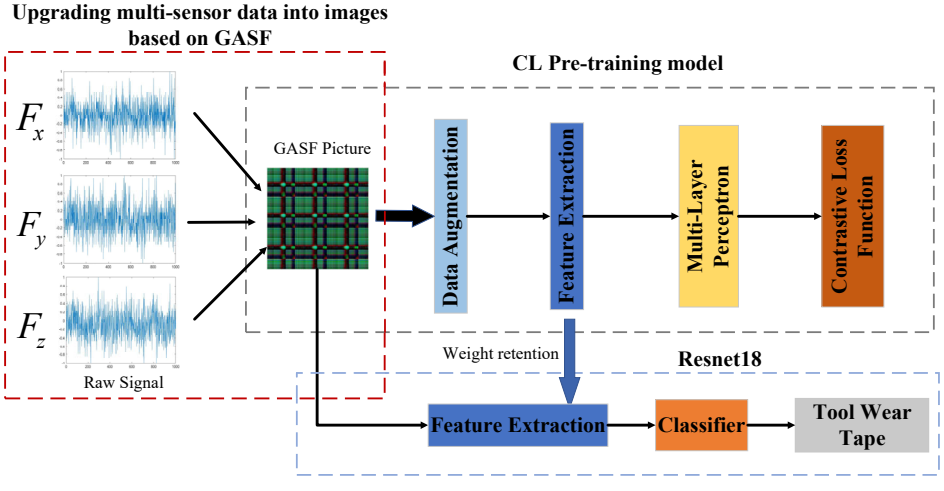

2.3 Proposed method

As shown in Figure 3, through the collected cutting force signal, the signal dimension is upgraded into grey image through GASF, the grey images obtained from the three signals are combined through the channel dimension to obtain a 3D colour image as the model input. This method uses a large number of unlabelled images to train a pre-training model based on CL, and the weight value of feature extraction in the pre-training model is used as the initial value of feature extraction in the classification model. Finally, a small batch of labelled datasets are used to fine tune the weight of feature extraction and dense layer, and the classification results are obtained.

3 Experimental investigations

3.1 Experimental setup

The TCM experimental setup is shown in Figure 4. The material of the work piece is AISI 1045 and the size is 300 mm 100 mm 80 mm, whose chemical properties are shown in Table 1. Each tool milled the work piece surface ten times, and the milling length of each time was 1.5m, including three climb milling and two conventional milling, and the sampling frequency is 12,000hz. Figure 5 shows the wear of the three edges of the first tool after the second, sixth and tenth milling stages.

According to the ISO3685-1977 standard, the wear amount of the tool is defined as the wear width VB of the flank of the tool. However, the one-dimensional measurement method cannot fully reflect the tool wear, so this study uses the flank wear area of the tool to measure the tool wear, and defines the maximum flank wear area of the three edges of the tool as the wear value of the milling cutter. According to the change trend of tool wear value in Figure 6, tool wear is divided into the following five categories in this paper: initial wear ($<0.1mm^2$), slight wear ($0.1mm^2 < x \leq 0.3mm^2$), stable wear ($0.3mm^2 < x \leq 0.5mm^2$), severe wear ($0.5mm^2 < x \leq 0.8mm^2$), failure ($> 0.8mm^2$). The classification results are shown in Table 3, assign the tool wear degree of these five categories to the data labels 1, 2, 3, 4 and 5.

Table 1 Chemical properties of work piece material

Carbon (%)	*Silicon (%)*	*Manganese (%)*	*Nickel (%)*	*Chromium (%)*	*Copper (%)*
0.42~0.50	0.17~0.37	0.50~0.80	＜0.30	＜0.25	＜0.25

In this paper, a total of 7 end mills were used for milling experiments, the cutting parameters for the milling method are shown in Table 4, the varied range of spindle speed is from 2300 *rpm* to 2500 *rpm*, the variation range of feed speed is from 400*mm/min* to 500*mm/min* and the variation range of cutting depth is from 0.4*mm* to 0.6*mm*, each milling cutter is tested from a new tool until the measured tool wear area is at least $0.8mm^2$, in this paper, 10 milling stages were carried out for each tool, and three cutting edges wear area values were recorded for each tool after each milling process.

Figure 4 The experimental setup (a) experimental platform (b) signal acquisition system (c) tool microscope (see online version for colours)

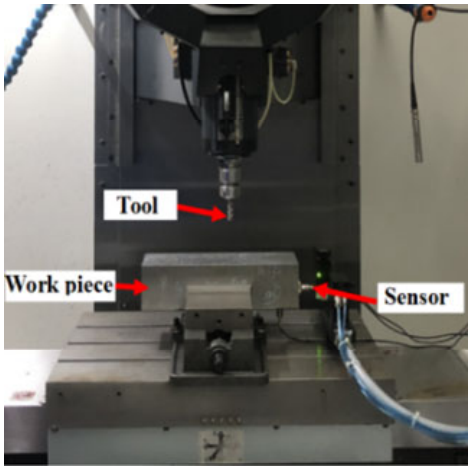

(a)

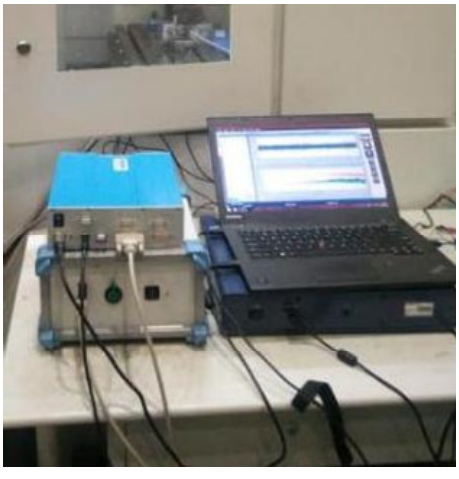

(b)

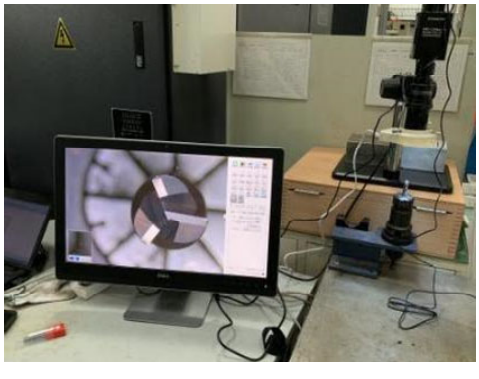

(c)

Table 2 Training parameters of CL pre-training model

Parameter	*Image size*	*Learning rate*	*Temperature parameter*	*Optimiser*	*Loss function*
Value	64×64×3	0.0005	0.1	Adam	Contrastive loss function

Table 3 Classification of tool wear status and range of wearable values

Tool category	*Tool wear value/mm²*	*Tool wear state*
1	[0, 0.1)	Initial wear
2	[0.1, 0.3)	Slight wear
3	[0.3, 0.5)	Stable wear
4	[0.5, 0.8)	Sharp wear
5	[0.8, +∞)	Failure

Figure 5 Tool wear images of different milling stages: (a) second milling stage (b) sixth milling stage (c) tenth milling stage

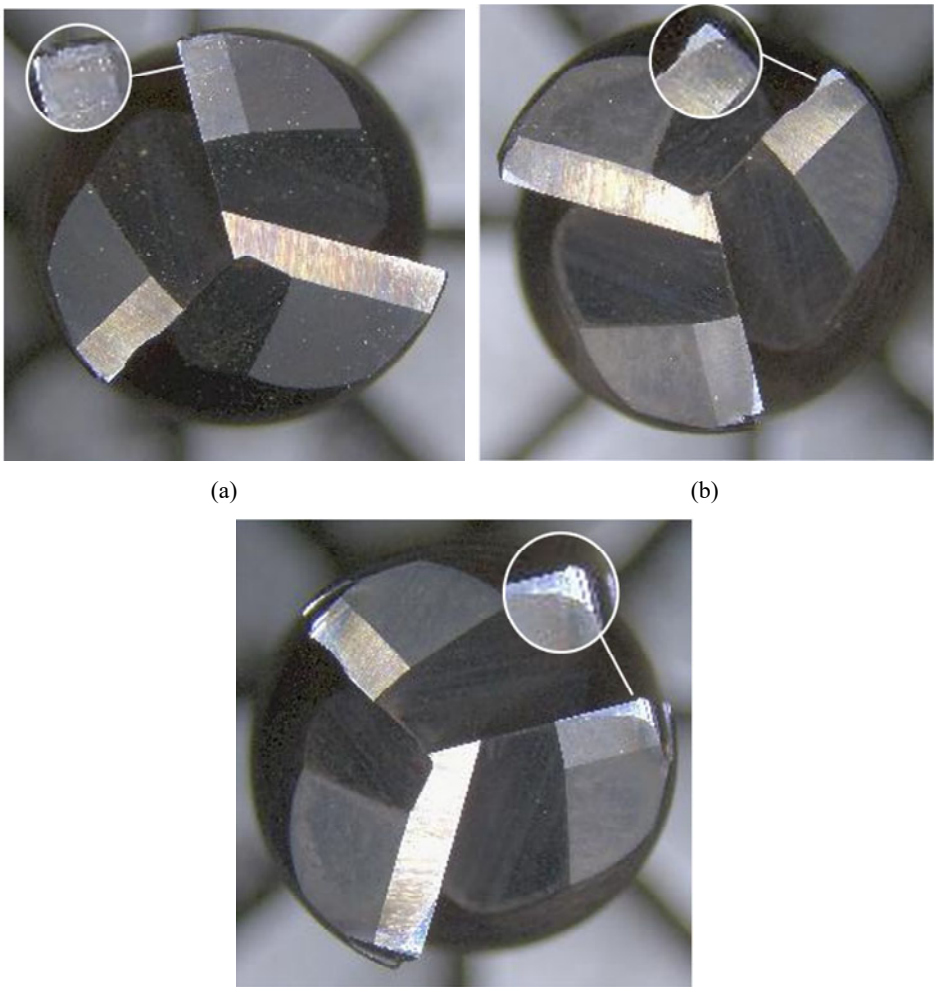

(a) (b)

(c)

Table 4 Machining parameters used in milling experiments

No.	*Speed (rpm)*	*Feed rate (mm/min)*	*Depth of cut (mm)*
1	2,300	400	0.4
2	2,300	450	0.5
3	2,300	500	0.6
4	2,400	450	0.4
5	2,400	500	0.5
6	2,400	400	0.6
7	2,500	400	0.6

Figure 6 Flank wear area of three cutting edges during milling (see online version for colours)

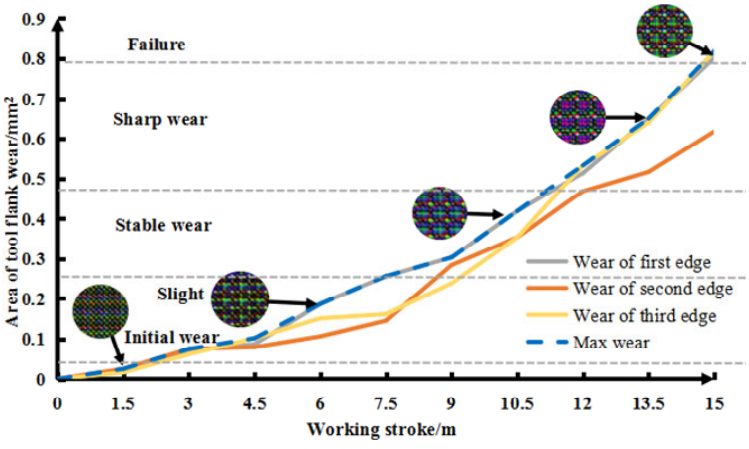

3.2 Results and analysis

In this experiment, each tool has a processing stroke of 10 units, therefore, the experimental results include 70 sets of cutting force signal data and the corresponding amount of wear at the milling stage, each sample contains the X, Y and Z axis cutting force signal, with 300 seconds in each direction and a total of 3,600,000 data points, and 1,000 signal points are defined by GASF to upgrade the dimension into an image as the image input of this study. Figure 7 shows the relationship between the five tool wear categories and the corresponding GASF dimension upgrade image.

Figure 7 Tool wear image and its corresponding GASF dimension upgrading image (see online version for colours)

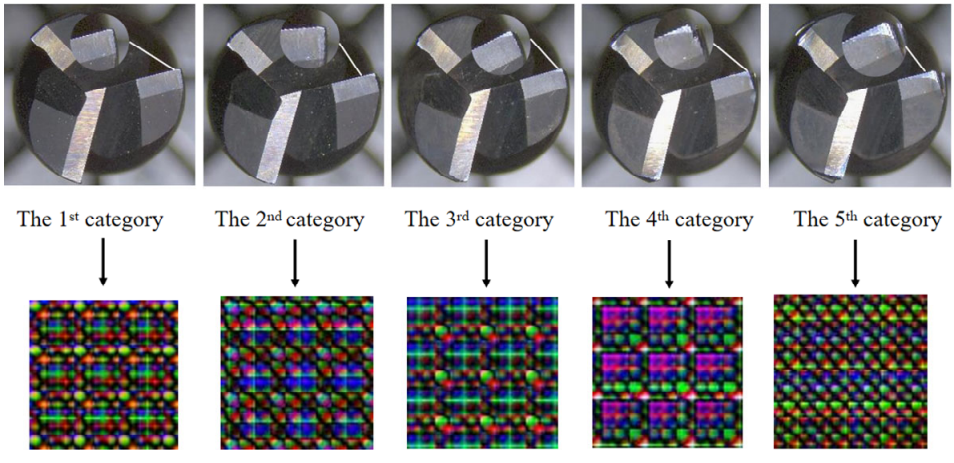

We will get a dataset of 7,000 samples per category, remove the labels of most samples from the dataset, and then obtain a dataset of 2,000 labelled samples (400 per class) and 33,000 unlabelled samples (6,600 per class), the labelled data is randomly divided into

half of the training set and half of the testing set (200 per class), the training set and the unlabelled dataset (1,000+33,000 samples) are applied to train the SimCLR pre-training model. Then, 50 samples of each class in the training set are selected as the validation set, and the remaining 150 samples of each class are used as the training set with sample sizes of 20, 30, 50, 100, and 150. The training set and the validation set are used to train the model, and the testing set is used to test the accuracy, and the average is repeated five times. These datasets are tested and compared in seven methods: GASF-CL, GASF-IM, GASF-ResNet 18 (no pre- training model), CL pre-trained model and ImageNet Pre-training model under short-time Fourier transform (Aafaq et al., 2019) (STFT-CL, STFT-IM), CL and ImageNet under the wavelet transform (Shao et al., 2018) (WT-CL ,WT-IM). The training parameters of CL pre-training model are shown in Table 2. Table 5 shows the classification results of the seven methods at different simple sizes.

Table 5 classification results of three methods under different sample sizes

No.	*T-20*	*T-30*	*T-50*	*T-100*	*T-150*
Labelled/class	20	30	50	100	150
STFT-IM	61.5%	63.2%	75.6%	84.1%	87.9%
STFT-CL	64.4%	66.8%	79.8%	87.2%	92.2%
WT-IM	62.3%	67.3%	74.5%	85.6%	89.6%
WT-CL	57.6%	62.2%	71.8%	80.5%	85.9%
GASF-ResNet18	44.9%	49.3%	59.4%	77.3%	85.2%
GASF-IM	63.5%	65.4%	73.8%	87.9%	91.8%
GASF-CL	81.5%	86.1%	92.3%	97.0%	98.0%

By taking the average of the results of the five repeated experiments of the seven methods in Table 5, it can be seen that when there are 150 pictures in each category in the training set, the test accuracy rate reaches 98%. Compared with the other six methods, this method has a 6% improvement in accuracy. When there are only 20 images in the training set, the classification results of the dataset obtained by the GASF-CL model method also have 81.5% test accuracy categories, which is much higher than other methods. It can be seen that the advantages of this method are more obvious when the sample size is smaller. Through the comparison of STFT-CL, WT-CL and GASF-CL, it can be seen that the GASF signal dimension enhancement method is more able to extract the deep features of the signal, coupled with CL pre-training method makes the trained model have better classification performance.

4 Conclusions

In this paper, the three directions of cutting force signals X, Y and Z are combined into a new dataset through the channel dimension, which solves the problem that the information obtained by a single channel is limited and there may be large errors, and improves the stability and robustness of the system. The CL pre-training model method is applied in the case of large sample size with a small proportion of label data, the self-supervised pre-training mode can also be used to make full use of the properties of

unlabelled data to learn the internal features of the image, and has a great effect compared with the traditional methods.

However, the CL method needs to utilise the positive and negative sample pairs of a large number of datasets to calculate the comparative loss function. It needs to be improved on the network model in the future, so that a slightly smaller number of datasets can achieve the same effect as the model obtained by the pre-training of large samples. In short, CL can better explore and improve, and make rational use of a large number of unlabelled datasets, which is still a problem worthy of research in the future.

Acknowledgements

This work was supported by the Wenzhou Key Innovation Project for Science and Technology of China under Grant ZG2021027.

References

Aafaq, N., Akhtar, N., Liu, W. et al. (2019) 'Spatio-temporal dynamics and semantic attribute enriched visual encoding for video captioning', *Proceedings of the IEEE/CVF Conference on Computer Vision and Pattern Recognition*, pp.12487–12496.

Chan, T., Jia, K., Gao, S. et al. (2014) 'Pcanet: A simple deep learning baseline for image classification?', arXiv preprint arXiv: 1404.3606[J].

Chauhan, S. and Vashishtha, G. (2021) 'Mutation-based arithmetic optimization algorithm for global optimization', *2021 International Conference on Intelligent Technologies* (CONIT), IEEE, pp.1–6.

Chauhan, S., Vashishtha, G. and Kumar, A. (2022) 'A symbiosis of arithmetic optimizer with slime mould algorithm for improving global optimization and conventional design problem', *The Journal of Supercomputing*, Vol. 78, No. 5, pp.6234–6274.

Chen, T., Kornblith, S., Norouzi, M. et al. (2020) 'A simple framework for contrastive learning of visual representations', *International Conference on Machine Learning,* PMLR, pp.1597–1607.

Gu, J.X., Albarbar, A., Sun, X. et al. (2021) 'Monitoring and diagnosing the natural deterioration of multi-stage helical gearboxes based on modulation signal bispectrum analysis of vibrations', *International Journal of Hydromechatronics*, Vol. 4, No. 4, pp.309–330.

Hadsell, R., Chopra, S. and LeCun, Y. (2006) 'Dimensionality reduction by learning an invariant mapping', *2006 IEEE Computer Society Conference on Computer Vision and Pattern Recognition* (CVPR'06), IEEE, Vol. 2, No. 6, pp.1735–1742.

Hahn, T.V. and Mechefske, C.K. (2021) 'Self-supervised learning for tool wear monitoring with a disentangled-variational-autoencoder', *International Journal of Hydromechatronics*, Vol. 1, No. 1, p.1.

Hahn, T.V. and Mechefske, C.K. (2021) 'Self-supervised learning for tool wear monitoring with a disentangled-variational-autoencoder', *International Journal of Hydromechatronics*, Vol. 4, No. 1, pp.69–98.

He, Z., Shao, H., Ding, Z. et al. (2021) 'Modified deep autoencoder driven by multisource parameters for fault transfer prognosis of aeroengine', *IEEE Transactions on Industrial Electronics*, Vol. 69, No. 1, pp.845–855.

He, Z., Shao, H., Zhong, X. et al. (2020) 'Ensemble transfer CNNs driven by multi-channel signals for fault diagnosis of rotating machinery cross working conditions', *Knowledge-Based Systems*, Vol. 207, No. 11, p.106396.

Higashi, N. and Iba, H. (2003) 'Particle swarm optimization with Gaussian mutation', *Proceedings of the 2003 IEEE Swarm Intelligence Symposium*, SIS'03 (Cat. No. 03EX706), IEEE, pp.72–79.

Hinton, G., Deng, L., Yu, D. et al. (2012) 'Deep neural networks for acoustic modeling in speech recognition: the shared views of four research groups', *IEEE Signal Processing Magazine*, Vol. 29, No. 6, pp.82–97.

Jafariasl, J., Ohadi, S., Seghier, M. et al. (2021) 'Accurate structural reliability analysis using an improved line-sampling-method-based slime mold algorithm', *ASCE-ASME Journal of Risk and Uncertainty in Engineering Systems Part A Civil Engineering*, Vol. 7, No. 2, pp.4021015–4021011.

Jiang, J., Guo, M. and Yang, S. (2021) 'Fault diagnosis method of rolling bearing based on GAF and DenseNet', *Industrial and Mining Automation*, *V.*, 47th, Vol. 305, No. 8, pp.84–89, DOI: 10.13272/j.issn.1671-251x.2021040095.

Klancnik, S., Ficko, M., Balic, J. et al. (2015) 'Computer vision-based approach to end mill tool monitoring', *International Journal of Simulation Modelling*, Vol. 14, No. 4, pp.571–583.

Lei, Z., Zhu, Q., Zhou, Y. et al. (2021) 'A GAPSO-enhanced extreme learning machine method for tool wear estimation in milling processes based on vibration signals', *International Journal of Precision Engineering and Manufacturing-Green Technology*, Vol. 8, No. 3, pp.745–759.

Li, Q., Li, P., Mao, K. et al. (2020) 'Improving convolutional neural network for text classification by recursive data pruning', *Neurocomputing*, Vol. 414, No. 11, pp.143–152.

Li, Z., Liu, R. and Wu, D. (2019) 'Data-driven smart manufacturing: tool wear monitoring with audio signals and machine learning', *Journal of Manufacturing Processes*, Vol. 48, No. 12, pp.66–76.

Ravindra, H.V., Srinivasa, Y.G. and Krishnamurthy, R. (1997) 'Acoustic emission for tool condition monitoring in metal cutting', *Wear*, Vol. 212, No. 1, pp.78–84.

Rehorn, A.G., Jiang, J. and Orban, P.E. (2005) 'State-of-the-art methods and results in tool condition monitoring: a review', *The International Journal of Advanced Manufacturing Technology*, Vol. 26, No. 7, pp.693–710.

Shao, S., McAleer, S., Yan, R. et al. (2018) 'Highly accurate machine fault diagnosis using deep transfer learning', *IEEE Transactions on Industrial Informatics*, Vol. 15, No. 4, pp.2446–2455.

Siddhpura, A. and Paurobally, R. (2013) 'A review of flank wear prediction methods for tool condition monitoring in a turning process', *The International Journal of Advanced Manufacturing Technology*, Vol. 65, No. 1, pp.371–393.

Vashishtha, G. and Kumar, R. (2022) 'Pelton wheel bucket fault diagnosis using improved Shannon entropy and expectation maximization principal component analysis', *Journal of Vibration Engineering and Technologies*, Vol. 10, No. 1, pp.335–349.

Vashishtha, G., Chauhan, S., Kumar, A. et al. (2022) 'An ameliorated African vulture optimization algorithm to diagnose the rolling bearing defects', *Measurement Science and Technology*, Vol. 33, No. 7, p.75013.

Vicente, J., Abellan-Nebot, F. et al. (2010) 'A review of machining monitoring systems based on artificial intelligence process models', *The International Journal of Advanced Manufacturing Technology*, Vol. 47, No. 3, pp.237–257.

Wang, J., Yan, J., Li, C. et al. (2019) 'Deep heterogeneous GRU model for predictive analytics in smart manufacturing: application to tool wear prediction', *Computers in Industry*, Vol. 111, No. 10, pp.1–14.

Wang, Z. and Oates, T. (2015) 'Imaging time-series to improve classification and imputation', *Proceedings of the 24th International Conference on Artificial Intelligence (IJCAI2015)*, AAAI Press, Buenos Aires, Argentina.

Wu, D., Jennings, C., Terpenny, J. et al. (2017) 'A comparative study on machine learning algorithms for smart manufacturing: tool wear prediction using random forests', *Journal of Manufacturing Science and Engineering*, Vol. 139, No. 7, p.071018.

Yu, W. and Zhao, F. (2019) 'Predictive study of ultra-low emissions from dual-fuel engine using artificial neural networks combined with genetic algorithm', *International Journal of Green Energy*, Vol. 16, No. 12, pp.938–946.

Zhang, L., Chen, Y., Wu, W. et al. (2021) 'Interpretable small sample learning based on contrastive constraints', *Computer Research and Development J.*, Vol. 58, No. 12, pp.2573–2584.

Zheng, W., Lin, R., Wang, J. et al. (2021) 'Power quality disturbance classification based on GAF and convolution neural network', *Protection and Control of Electric Power System*, Vol. 581, No. 11, pp.97–104, DOI: 10.19783/j.cnki.pspc.200997.

Zhou, Y., Sun, B. and Sun, W. (2020a) 'A tool condition monitoring method based on two-layer angle kernel extreme learning machine and binary differential evolution for milling', *Measurement*, Vol. 166, No. 12, p.108186.

Zhou, Y., Sun, B., Sun, W. et al. (2020b) 'Tool wear condition monitoring based on a two-layer angle kernel extreme learning machine using sound sensor for milling process', *Journal of Intelligent Manufacturing*, Vol. 31, No. 1, pp.247–258.

Zhou, Y., Zhi, G., Chen, W. et al. (2022) 'A new tool wear condition monitoring method based on deep learning under small samples', *Measurement*, Vol. 189, No. 2, p.110622.

Zhu, Q., Sun, B., Zhou, Y. et al. (2021) 'Sample augmentation for intelligent milling tool wear condition monitoring using numerical simulation and generative adversarial network', *IEEE Transactions on Instrumentation and Measurement*, Vol. 70, No. 5, pp.1–10.